Catalysis Letters Vol. 108, Nos. 3–4, May 2006 (© 2006)
DOI: 10.1007/s10562-006-0040-z

Reducibility of $Ce_{1-x}Zr_xO_2$: origin of enhanced oxygen storage capacity

Gargi Dutta,[a] Umesh V. Waghmare,[a] Tinku Baidya,[b] M.S. Hegde,[b,*] K.R. Priolkar,[c] and P.R. Sarode[c]

[a]*Theoretical Sciences Unit, Jawaharlal Nehru Centre for Advanced Scientific Research, Jakkur Campus, Bangalore 560 064, India*
[b]*Solid State and Structural Chemistry Unit, Indian Institute of Science, Bangalore 560 012, India*
[c]*Department of Physics, Goa University, Taleigao Plateau, Goa 403 206, India*

Received 3 January 2006; accepted 25 January 2006

We combine first-principles calculations with EXAFS studies to investigate the origin of high oxygen storage capacity in ceria-zirconia solid solution, prepared by solution combustion method. We find that nanocrystalline $Ce_{0.5}Zr_{0.5}O_2$ can be reduced to $Ce_{0.5}Zr_{0.5}O_{1.57}$ by H_2 upto 850 °C with an OSC of 65 cc/gm which is extremely high. Calculated local atomic-scale structure reveals the presence of long and short bonds resulting in four-fold coordination of the cations, confirmed by the EXAFS studies. Bond valence analysis of the microscopic structure and energetics is used to evaluate the strength of binding of different oxide ions and vacancies. We find the presence of strongly and weakly bound oxygens, of which the latter are responsible for the higher oxygen storage capacity in the mixed oxides than in the pure CeO_2.

KEY WORDS: biomimetic oxidation catalysts; biotransformation; D-limonene; porphyrin; uv–vis spectroscopy; photooxidation.

1. Introduction

Amount of oxygen that can be released under reducing condition and to uptake it under oxidizing condition is called oxygen storage capacity (OSC) [1,2]. Temperature programmed reduction (TPR) by H_2 is generally employed to estimate OSC. The mechanism of CeO_2–Ce_2O_3 transition associated with oxygen vacancy formation was explained on the basis of first-principles calculations as a possible reason behind the high OSC of ceria [3]. Even though ZrO_2 cannot be reduced by CO or H_2, OSC was enhanced in the $Ce_{1-x}Zr_xO_2$ solid solution [4–6]. This means, in the solid solution, Ce can be reduced lot more easily compared to pure CeO_2. Because of its importance in auto exhaust catalysis, several studies exist in the literature to explain this observation [7–9]. It was suggested that the availability of free oxygen is increased by the transport of bulk oxygen to surface [10]. Later, movement of oxide ions from the tetrahedral sites to the vacant octahedral sites was suggested to be one of possibilities which can enhance OSC [11]. A common observation is that the X-ray diffraction lines of $Ce_{1-x}Zr_xO_2$ are much broader in the solid solution. This is generally attributed to the decrease in size of crystallites and therefore higher OSC was attributed to larger surface area of $Ce_{1-x}Zr_xO_2$. It is also possible that the local coordination around Zr in $Ce_{1-x}Zr_xO_2$ is different from the ideal eight-fold coordination of Ce in CeO_2, which can lead to broadening of X-ray lines. EXAFS studies have revealed 4 + 4 coordination for Zr in $Ce_{1-x}Zr_xO_2$ [12,13]. Atomistic and first-principles calculations have been valuable in studies of ceria, its surfaces [14] and interaction with Hydrogen [15]. Important study has been done on the role of oxygen vacancies on ceria surfaces in the oxidation of carbon monoxide [16]. Higher OSC or increased reducibility of CeO_2 in the CeO_2–ZrO_2 solid solution has not been satisfactorily explained in the earlier studies, as referred above. Here we report H_2/TPR of $Ce_{1-x}Zr_xO_2$ and a first principles structural study of solid solutions. Theoretically determined structure of $Ce_{1-x}Zr_xO_2$ is compared with results of EXAFS. We show that oxygen sublattice is significantly distorted leading to destabilization of oxide ions in terms of Ce–O, Zr–O distances.

2. Methods

2.1. Experiment

$Ce_{1-x}Zr_xO_2$ has been prepared by solution combustion method. Stoichiometric amounts of ceric ammonium nitrate, zirconium nitrate and glycine were taken in a glass vessel; the salts were dissolved into solution by adding minimum amount of water. The solution was heated rapidly at 350 °C. At the point of complete water evaporation, the material ignites into a flame reaching a temperature of above 900 °C. After the combustion is complete, the sample cools to 350 °C in about 1 min. The product was fine powder of $Ce_{1-x}Zr_xO_2$ which was analysed. Hydrogen uptake was measured by temperature programmed reduction with 5% H_2 in Ar from 30 °C to 850 °C. Volume of H_2 taken up for reduction is calibrated against that of CuO. The chemical reactions

*To whom correspondence should be addressed.
E-mail: mshegde@sscu.iisc.ernet.in

for the formation of CeO_2 and $Ce_{1-x}Zr_xO_2$ can be written as follows:

(a) $3(NH_4)_2Ce(NO_3)_6 + 8C_2H_5NO_2 = 3CeO_2 + 10N_2 + 16CO_2 + 32H_2O$

(b) $9(1-x)(NH_4)_2Ce(NO_3)_6 + 9xZr(NO_3)_4 + 20C_2H_5NO_2 + 4(1-x)C_2H_5NO_2 = 9Ce_{1-x}Zr_xO_2 + 40CO_2 + 8(1-x)CO_2 + 28N_2 + 20(1-x)N_2 + 50H_2O + 46(1-x)H_2O$

EXAFS at the Zr K-edge were recorded in transmission mode at the EXAFS-1 Beamline at Elettra Synchrotron Source using Si(111) as monochromator. The incident and transmitted flux was measured using ionization chambers filled with a mixture of N_2 and Ar and pure Ar gases respectively. For the measurements, absorbers were prepared in the form of self-supporting pellets (~40 mg) of about 10 mm diameter. The amount of sample was zalculated such that total absorption coefficient (μx) after the edge was around than 2.5. The energy was calibrated with respect to Cu K-edge in Cu metal. Three scans of each were recorded in the energy interval 17,750–19,000 eV in steps of 5 eV in the pre-edge region (~200 eV),and 2 eV for the rest of the scan. Data analysis was done using the open source IFEFFIT analysis package developed by Matt Newville at the University of Chicago.

2.2. Theory

Our total energy calculations are based on density functional theory (DFT) with a local density approximation (LDA) to the exchange correlation energy of electrons. While the LDA + U type of corrections are known to be important in reduced form of ceria [17], we are mainly interested in the atomic structure which is expected to be less sensitive to these corrections. Interaction between valence electrons and ionic cores is treated using first-principles ultra-soft pseudopotentials [18] and single particle wavefunctions (density) were represented with a plane wave basis with an energy cutoff of 30 Ry (150 Ry). Semi-core states of Ce and Zr are included in the valence. We use PWSCF [19] implementation of DFT for these calculations. Zr substitution in CeO_2 is treated using periodic supercells of up to 8 formula units of CeO_2 with Ce atoms replaced with Zr according to different concentrations of Zr substitution. Internal structure in each case was optimized to minimize the total energy using the Broyden, Fletcher, Goldfarb, Shanno (BFGS)-based method [20].

Integrals over the Brillouin zone were sampled on 4×4×4 k-point Monkhorst–Pack [21] mesh for pure CeO_2, pure ZrO_2 and $Ce_{0.75}Zr_{0.25}O_2$ which were simulated with a cubic unit cell with four formula units of MO_2 (M = metal ion). For $Ce_{0.875}Zr_{0.125}O_2$ and $Ce_{0.50}Zr_{0.50}O_2$ we used a tetragonal supercell (doubled in the *ab*-plane, $c/a = 0.71$) with eight formula units and Brillouin zone was sampled on a 3×3×4 Monkhorst–Pack [21] k-point mesh.

The bond distances determined from the optimized structures are used to calculate valencies of metal ions following the bond valence method [22]. Bond valence s is defined as: (a) $s = (R/R_o)^{-N}$ (for Zr–O bonds) and (b) $s = exp[-(R-R_o)/B]$ (for Ce–O bonds), where R is the bond length, R_o is the length of a bond of unit valence, N and B are fitted parameters. For Ce–O and Zr–O bonds, $R_o^{\mathrm{LDA}} = R_o \frac{a^{\mathrm{LDA}}}{a^{\mathrm{exp}}}$, where a^{LDA} is the lattice constant from our theoretical calculations and a^{exp} is the experimental lattice constant. The atomic valence V is obtained by summing the bond valencies associated with a particular ion given by $V = \mathrm{T}_i s_i$.

3. Results

As seen from the X-ray diffraction patterns of $Ce_{1-x}Zr_xO_2$ ($x = 0.0$–0.5) (given in figure 1), the oxides crystallize in fluorite structure. On Zr substitution, X-ray line widths become broader compared to pure CeO_2. Lattice parameters of the oxides have been determined and a decrease in 'a' for the Zr substituted oxides is observed as expected (see table 1). The average crystallite size of $Ce_{0.75}Zr_{0.25}O_2$ obtained from Scherrer's formula is 18 nm. Hydrogen uptake as a function of temperature is shown in figure 2. Note, the y scales are different for the different samples. For pure CeO_2, the total H_2 uptake upto 850 °C corresponds to the reduction of CeO_2 to $CeO_{1.92}$. $Ce_{0.75}Zr_{0.25}O_2$ gets reduced to $Ce_{0.75}Zr_{0.25}O_{1.70}$. $Ce_{0.5}Zr_{0.5}O_2$ is reduced to $Ce_{0.5}Zr_{0.5}O_{1.57}$.

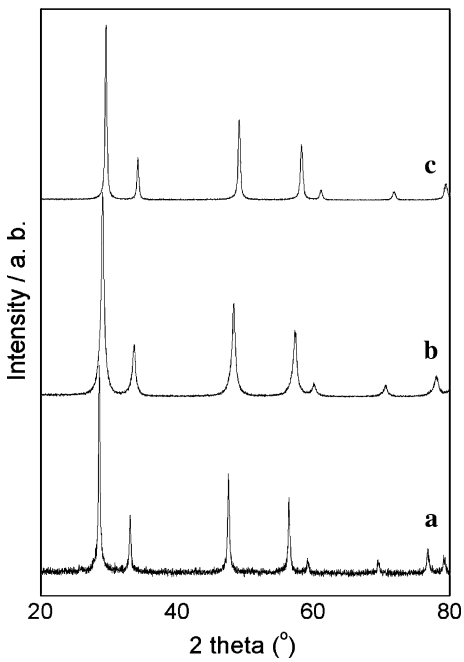

Figure 1. XRD pattern of (a) CeO_2, (b) $Ce_{0.75}Zr_{0.25}O_2$, (c) $Ce_{0.5}Zr_{0.5}O_2$.

Table 1
Lattice constants 'a' in Å

Oxide	Calculation	Experiment
CeO_2	5.46	5.41
ZrO_2	5.03	5.09
$Ce_{0.875}Zr_{0.125}O_2$	5.43	5.36
$Ce_{0.75}Zr_{0.25}O_2$	5.40	5.32
$Ce_{0.50}Zr_{0.50}O_2$	5.26	5.27

Zr k-edge EXAFS in $Ce_{0.5}\,Zr_{0.5}\,O_2$ and $Ce_{0.7}\,Zr_{0.3}\,O_2$ was Fourier transformed (FT) in the k-range 2 $Å^{-1}$-12 $Å^{-1}$ with k^2 weighting. The resulting magnitudes of FT in the range 1 Å–4 Å along with the back transformed data are presented in figure 3. The magnitude of FT shows a strong peak at about 2.1 Å corresponding to Zr–O correlations. Some more peaks are also seen in the range 3 Å corresponding to Zr–O correlations. Some more peaks are also seen in the range 3 Å–4 Å which could be ascribed to Zr–Zr(Ce) and Zr–O coordination shells.

The first peak was fitted using Zr–O correlation with different combination of coordination numbers. In the first instance, a single shell fitting was performed. This fitting gave a coordination number of 3.8 at 2.18 Å. However, 8 oxygens surround the metal ion in the fluorite structure. Hence coordination of 3.8 is not satisfactory. A two-shell fitting was carried out with fixed coordination numbers. Three models were used to fit the data. In all the cases the total coordination number was 8 but was arrived at through different combinations

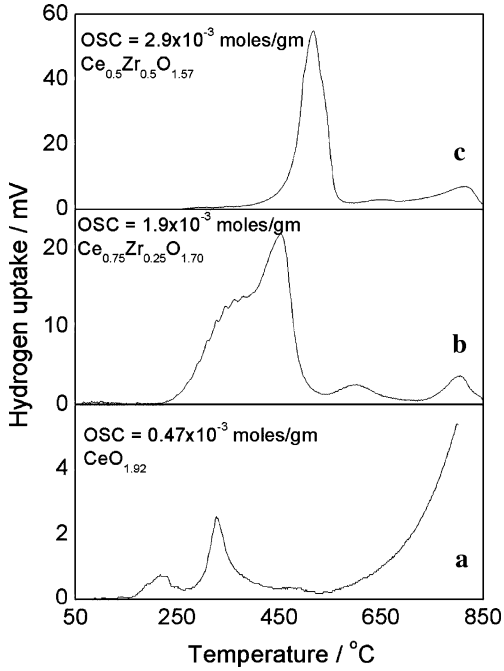

Figure 2. H_2 uptake for CeO_2 and $Ce_{1-x}Zr_xO_2$.

namely, 6 + 2, 4 + 4 and 4 + 2 + 2. The results of all these fittings are presented in table 2. Vlaic *et al.* [12] have used such combinations for the analysis of their Zr K EXAFS in $Rh/Ce_{0.5}Zr_{0.5}O_2$. In case of 6 + 2 combination, the Zr–O bond distances obtained were 2.20 and 2.52 Å. The first distance of 2.20 Å is higher than Zr–O

Table 2
Local coordination in $Ce_{0.5}Zr_{0.5}O_2$ and $Ce_{0.7}Zr_{0.3}O_2$ determined from Zr K-edge EXAFS (C.N. – coordination number was kept fixed in all the fitting iterations, bond distance R in Å)

Sample	Coordination Shell	C.N.	R	σ^2	R (Theory)
$Ce_{0.5}Zr_{0.5}O_2$	Zr–O	6	2.20 ± 0.01	0.008 ± 0.002	
		2	2.52 ± 0.20	0.040 ± 0.010	
		4	2.17 ± 0.03	0.006 ± 0.002	2.13
		4	2.30 ± 0.04	0.019 ± 0.006	2.32
		4	2.15 ± 0.01	0.002 ± 0.002	
		2	2.31 ± 0.02	−0.0006 ± 0.003	
		2	2.64 ± 0.20	0.02 ± 0.01	
	Zr–Zr	6	3.65 ± 0.04	0.012 ± 0.004	3.68
	Zr–Ce	6	3.71 ± 0.02	0.007 ± 0.002	3.72
	Zr–O	24	4.42 ± 0.04	0.024 ± 0.008	
$Ce_{0.7}Zr_{0.3}O_2$	Zr–O	6	2.19 ± 0.01	0.008 ± 0.002	
		2	2.60 ± 0.30	0.040 ± 0.010	
		4	2.17 ± 0.02	0.006 ± 0.002	
		4	2.30 ± 0.04	0.019 ± 0.006	
		4	2.15 ± 0.01	0.002 ± 0.002	
		2	2.30 ± 0.02	−0.0007 ± 0.003	
		2	2.65 ± 0.20	0.02 ± 0.01	
	Zr–Zr	3.6	3.66 ± 0.05	0.010 ± 0.005	
	Zr–Ce	8.4	3.71 ± 0.02	0.010 ± 0.002	
	Zr–O	24	4.41 ± 0.02	0.021 ± 0.004	

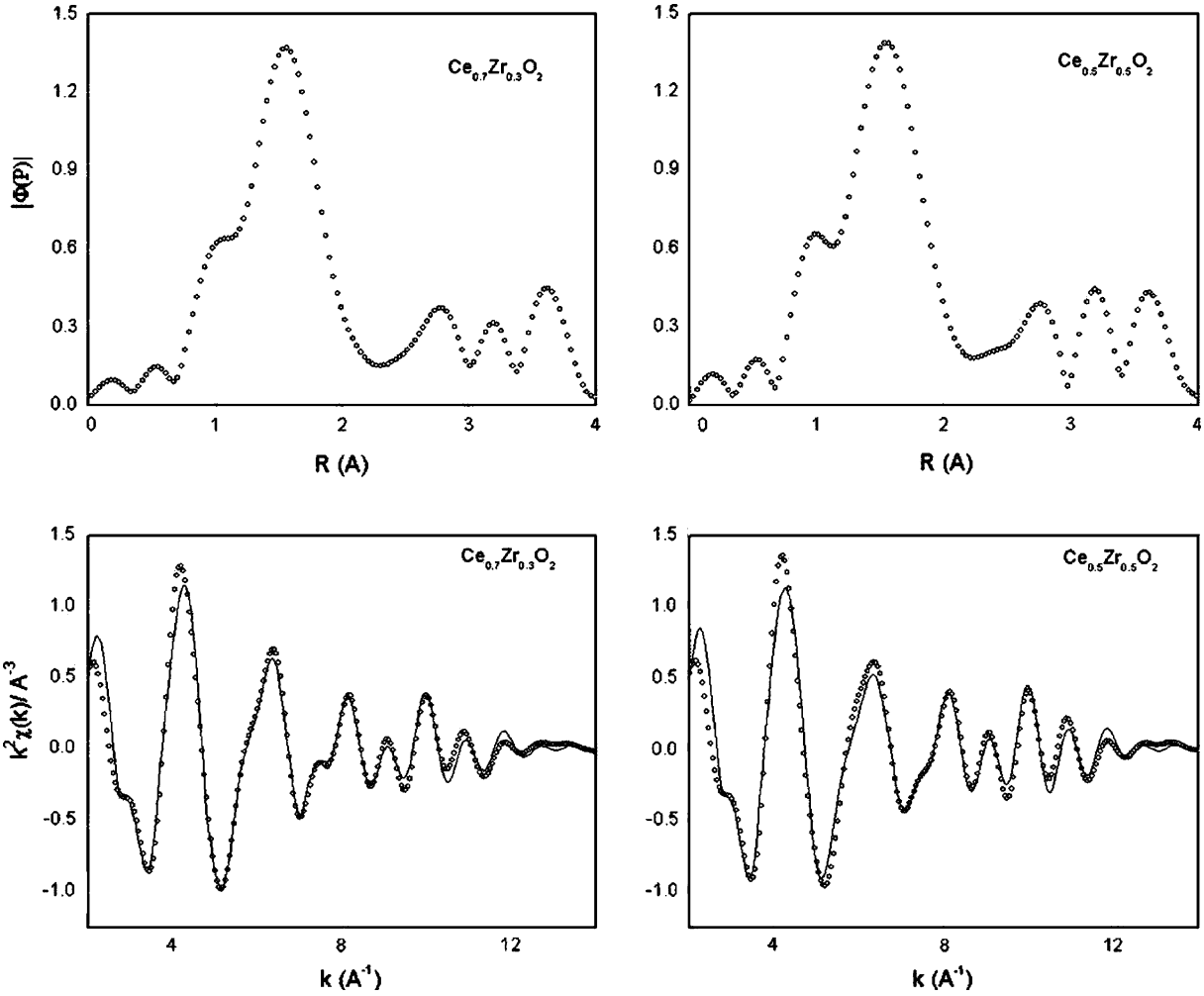

Figure 3. EXAFS analysis.

distance expected in pure ZrO_2 and the second distance is quite long. Such a long distance has not been reported earlier. Vlaic et al. have reported a Zr–O bond at 2.6 Å in Rh/$Ce_{0.5}Zr_{0.5}O_2$ with coordination number 2 in their 4, 2 and 2 model. In case of 4 + 4 model, the Zr–O distances obtained were 2.17 and 2.30 Å. As can be seen the first distance closely matches with Zr–O distance in ZrO_2 and the second one is close to the Ce–O distance in pure CeO_2. In the case of a three-shell fit with 4 + 2 + 2 coordination numbers the distances obtained were 2.15, 2.31 and 2.64 Å, respectively. But as can be seen from table 2 the σ^2 for the correlation at 2.31 Å is negative. Thus from the EXAFS analysis of the first peak 4 + 4 coordination of oxide ions around Zr ion gives the best fit. Further the second shell correlations namely: Zr–Zr, Zr–Ce and Zr–O were included in the fitting. The parameters obtained are presented in table 2 and the complete fitting in the back-transformed space is shown in figure 3. The data is fitted for the three different coordinations of $Ce_{0.7}Zr_{0.3}O_2$ also. Clearly, 4 + 4 coordination of oxygen around Zr is better than 6 + 2 or 4 + 2 + 2 coordinations. The fitting is good as can be seen from the figure. The bond lengths and debye waller factors remain almost same irrespective of oxygen coordination in the first shell. Similar 4 + 4 coordination for Zr ion is found by Lemaux *et al.* [13].

The lattice constants determined from first principles calculations are within the typical DFT errors with respect to their experimental values (see table 1). The local coordination of cations in the optimised structure of $Ce_{0.75}Zr_{0.25}O_2$ is shown in figure 4(a). As labelled in the figure, oxygens O1, O3, O6, O8 form short Zr–O bonds and while oxygens O2, O4, O5, O7 form long Zr–O bonds. Four of the eight nearest neighbour oxide ions come closer to Zr ion, resulting in coordination of four with average distance of 2.03 Å. O3 forms a short bond with Zr and a long bond with Ce, while O7 forms a long bond with Zr and a short bond with Ce. Hence oxygens farther from the Zr ion are closer to the Ce ion and vice versa. The average distance of the four nearest oxygens around Ce ion is 2.26 Å. The average Zr–O, Zr–Zr and Zr–Ce distances obtained from the calculation are given in table 2. As can be seen from the table, the calculated

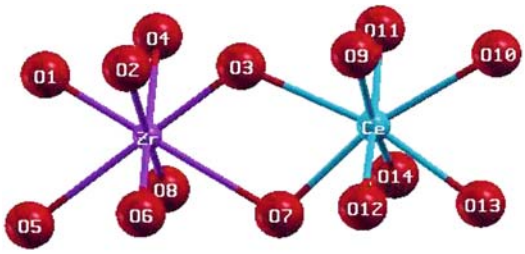

(a)

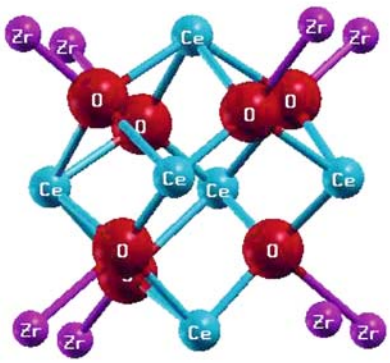

(b)

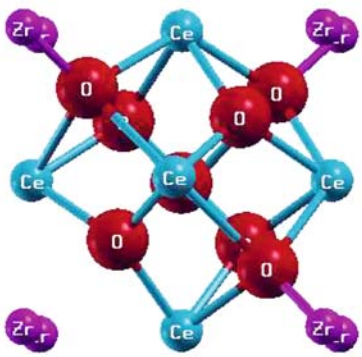

(c)

Figure 4. (a) $Ce_{0.75}Zr_{0.25}O_2$, showing the coordination around Zr and Ce ions. (b) $Ce_{0.75}Zr_{0.25}O_{1.75}$, with an oxygen vacancy in the tetrahedral position. (c) Initial configuration of $Ce_{0.75}Zr_{0.25}O_2$ with an oxygen vacancy in the tetrahedral position and an oxygen in the octahedral hole.

values agree quite well with the 4+4 coordination model in the EXAFS experiment.

With access to local structural details, we did bond valence analysis to uncover the cause for the enhanced observed OSC. The parameters used in the bond valence calculation [22] are given in table 3. For pure CeO_2, the average valency of Ce is 3.97 and that of an oxygen is 1.99. For pure ZrO_2, two types of average valencies of

Table 3
Parameters used in bond valence calculation, all distances in Å

Type of bond	R_o	R_o^{LDA}	Constant
Ce–O	2.12	2.14	$B=0.33$
Zr–O	1.95	1.93	$N=6.00$

Table 4
Calculated valencies of oxide ions in ceria-zirconia solid solution

Mixed oxides	Oxygen valency	Bonds made by oxygen
$Ce_{0.875}Zr_{0.125}O_2$	2.12	3 Ce–O short bonds, 1 Zr–O long bond
	2.09	3 Ce–O long bonds, 1 Ce–O short bond
	2.03	3 Ce–O short bonds, 1 Ce–O long bond
	1.79	3 Ce–O long bonds, 1 Zr–O short bond
$Ce_{0.75}Zr_{0.25}O_2$	2.19	3 Ce–O short bonds, 1 Zr–O long bond
	1.86	3 Ce–O long bonds, 1 Zr–O short bond
$Ce_{0.75}Zr_{0.25}O_{1.75}$	2.34	3 Ce–O short bonds, 1 Zr–O long bond
	2.17	3 Ce–O short bonds, 1 Zr–O long bond
	1.87	3 Ce–O long bonds, 1 Zr–O short bond
$Ce_{0.50}Zr_{0.50}O_2$	2.19	2 Ce–O short bonds, 1 Ce–O long bond, 1 Zr–O long bond
	2.03	2 Ce–O long bonds, 1 Ce–O short bond, 1 Zr–O short bond
	1.97	2 Zr–O long bonds, 1 Ce–O short bond, 1 Zr–O short bond
	1.76	2 Zr–O short bonds, 1 Ce–O long bond, 1 Zr–O long bond

Zr are 4.11 and 3.90. The average oxygen valency is 1.98. Thus, the metal and oxygen valencies in pure oxides are close to the expected values of 4.0 and 2.0, respectively.

In $Ce_{0.75}Zr_{0.25}O_2$, as given in table 4, the oxygens with three Ce–O long bonds and one Zr–O short bond have valency lower than 2.0 and the oxygens with 3 Ce–O short bonds and 1 Zr–O long bond have valency greater than 2.0. For other concentrations of Zr also, the oxygens can be grouped into the two types as in $Ce_{0.75}Zr_{0.25}O_2$. The increase in oxygen valencies above 2.0 shows that these oxygens are strongly bonded. The oxygens whose valencies are lower than 2.0, are weakly bonded. The average Zr valencies in $Ce_{0.50}Zr_{0.50}O_2$ $Ce_{0.75}Zr_{0.25}O_2$ and $Ce_{0.875}Zr_{0.125}O_2$ are 3.54, 3.62 and 3.47, respectively. The average Ce valencies in $Ce_{0.50}Zr_{0.50}O_2$, $Ce_{0.75}Zr_{0.25}O_2$ and $Ce_{0.875}Zr_{0.125}O_2$ are 4.41, 4.19 and 4.10, respectively.

It is noteworthy that the valency of the weakly bonded oxygen in $Ce_{0.75}Zr_{0.25}O_2$ is 1.86 and that of $Ce_{0.75}Zr_{0.25}O_{1.75}$ is 1.87 (vacancy introduced mixed oxide will be discussed later). In $Ba_2YCu_3O_7$, [23] the valency of the oxygen in the Cu–O plane is about 1.87 and this particular oxygen is weakly bonded with the effect that it can be desorbed at about 400 °C and is available as free oxygen. Therefore, in ceria-zirconia solid solution, oxide ions having valency close to 1.87

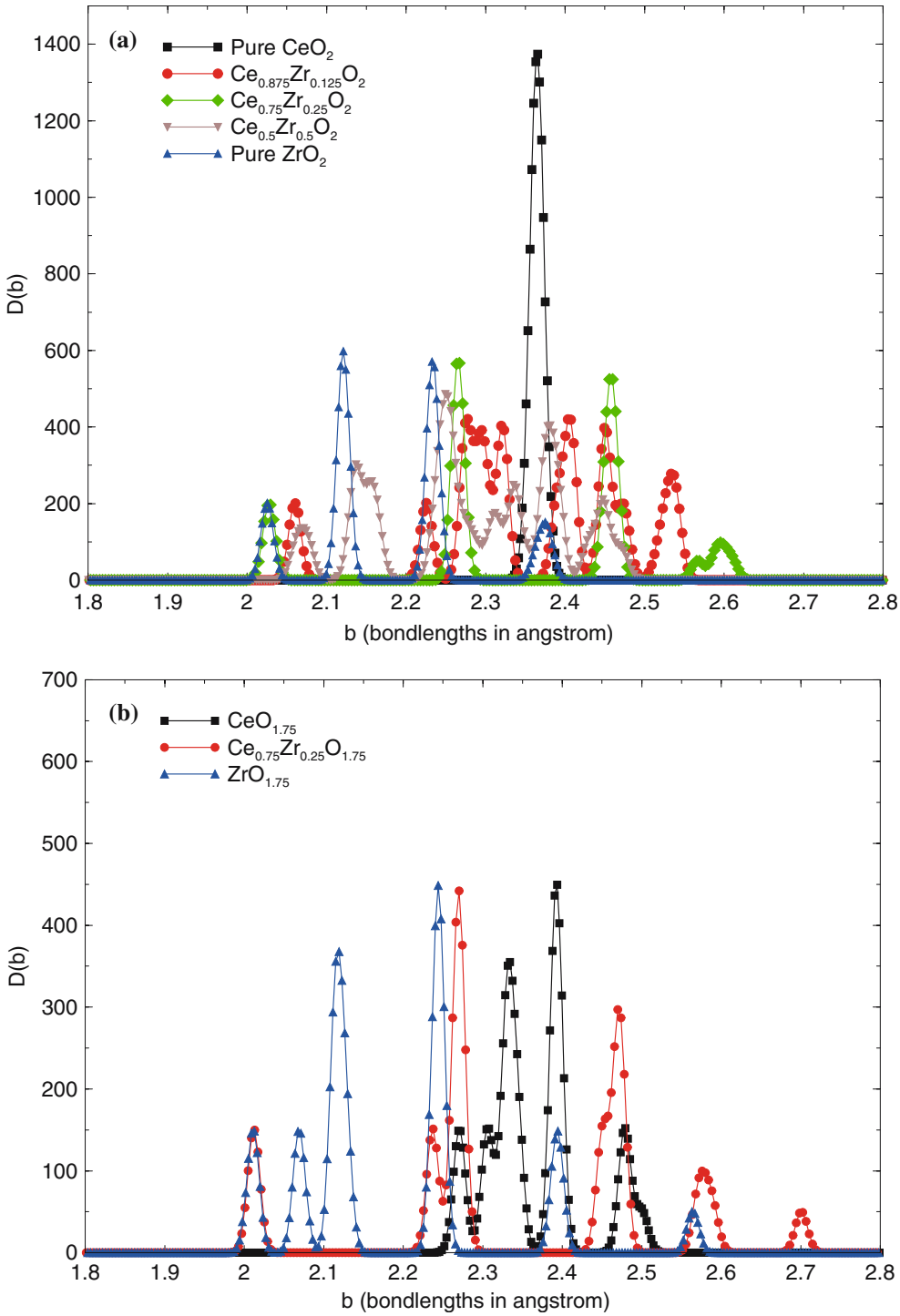

Figure 5. Distribution of cation – oxygen bond lengths in (a) CeO_2–ZrO_2 (b) Vacancy introduced CeO_2–ZrO_2.

and below are weakly bound and they can be reduced by H_2 or CO.

Distribution of cation to oxygen distances given in figure 5(a) shows the presence of a single Ce–O bond length in pure CeO_2 at 2.36 Å. On Zr substitution, bond lengths can be divided into two categories short and long, where the short category falls below 2.36 Å, and the long category falls above 2.36 Å. In $Ce_{0.875}Zr_{0.125}O_2$, three types of short and three types of long bonds are found. In $Ce_{0.75}Zr_{0.25}O_2$, two types of short and two types of long bonds are found. In pure ZrO_2, even though there are short and long bonds, all the bond lengths fall under the short category. The long bonds are weaker and the short bonds are stronger, hence availability of longer bonds in Zr doped CeO_2 lead to higher oxygen storage capacity than pure CeO_2 and pure ZrO_2.

Table 5
Bond lengths in ceria-zirconia (Å)

Oxide	bond lengths
Pure CeO_2	2.36 (Ce–O)
$CeO_{1.75}$	2.27, 2.33, 2.39, 2.48 (Ce–O)
$Ce_{0.875}Zr_{0.125}O_2$	2.22, (2.28, 2.29, 2.32), 2.40, 2.45 (Ce–O)
	2.06 (Zr–O)
	2.53 (mixed Ce–O and Zr–O)
$Ce_{0.75}Zr_{0.25}O_2$	2.26, 2.45 (Ce–O)
	2.03, 2.59 (Zr–O)
$Ce_{0.75}Zr_{0.25}O_{1.75}$	(2.24, 2.27), 2.47 (Ce–O)
	2.01, 2.58, 2.70 (Zr–O)
$Ce_{0.50}Zr_{0.50}O_2$	2.25, 2.44 (Ce–O)
	2.07, 2.14 (Zr–O)
	2.33, 2.38 (mixed Ce–O and Zr–O)
Pure ZrO_2	2.02, 2.12, 2.23, 2.37 (Zr–O)
$ZrO_{1.75}$	2.01, 2.07, 2.12, 2.24, 2.39, 2.56 (Zr–O)

The bond lengths inside parentheses correspond to the peaks which are closely grouped in the bond length distribution plots (figure 5).

Table 6
Strength of bonds in $Ce_{0.75}Zr_{0.25}O_2$: relative difference in bonding energy with respect to Ce–O bond in pure CeO_2 ('–' denotes a weaker bond and '+' denotes a stronger bond)

Type of bond	Relative difference in bond strengths (%)
Ce–O (long)	−28.72
Ce–O (short)	+28.60
Zr–O (long)	−85.71
Zr–O (short)	−37.94
Ce–O	0

Note that a Zr–O bond in pure ZrO_2 is 60 % weaker than the Ce–O bond in pure CeO_2.

Table 7
Relative binding energy (BE) of different type of oxygens in $Ce_{0.75}Zr_{0.25}O_2$ with respect to an oxygen in pure CeO_2, where each oxygen form four bonds with cations

Oxide	Type of oxygen	% Change of BE	No. of each type
Pure CeO_2	single type	0.00	8
$Ce_{0.75}Zr_{0.25}O_2$	Type 1 (strong)	+0.02	4
	Type 2 (weak)	−31.02	4

'–' denotes a weak oxygen and '+' denotes a strong oxygen.

Table 5 show the average value of bond lengths in Zr substituted CeO_2. Thus from the bond valence analysis, two type of oxygens can be identified: type 1 (strong), type 2 (weak).

The total cohesive energy E can be expressed in terms of bond energy $\epsilon(b)$: $\int \epsilon(b)\ D(b)\ db = E$, $D(b)$ being the distribution of bond-lengths or the bond-length density. To determine energies of short and long bonds in $Ce_{1-x}Zr_xO_2$, we assume the following simple relation: $\frac{E_{\text{type1}}}{E_{\text{type2}}} = \frac{\text{av}(s_{\text{type1}})}{\text{av}(s_{\text{type2}})}$, where av($s$) is the average bond valence of a type of bond. According to the bond valence theory, valence of an atom is a measure of its involvement in bonding [22]. As the valence of an atom is the sum of its individual bond valences, it is reasonable to assume that more is the bond valence, the stronger is the bond and vice versa.

The relative bonding energies in $Ce_{0.75}Zr_{0.25}O_2$ given in table 6 bear that, Ce–O (long), Zr–O (long), Zr–O (short) bonds are weaker than the pure Ce–O bond. We have showed the % difference in the bonding energies with respect to pure Ce–O bond because their absolute values are typically overestimated in LDA calculations.

The binding energy of different type of oxygens is obtained by summing up of individual bond energies. The relative binding energy of oxygens in Zr substituted CeO_2 is given in table 7. For pure CeO_2, we have a single type of oxygen, in which each oxygen forms four bonds with Ce. For $Ce_{0.75}Zr_{0.25}O_2$, the binding energy of an oxygen with 3 Ce–O short bonds and 1 Zr–O long bond is given by type 1 and have binding energy more than that of an oxygen in pure CeO_2. Type 2, in which oxygen has 3 Ce–O long bonds and 1 Zr–O short bond are weakly bound than an oxygen in pure CeO_2. Our analysis of bond-strengths is consistent with the result that cohesive energy of $Ce_{0.75}Zr_{0.25}O_2$ is 15.53% smaller than pure CeO_2.

To probe further the OSC of mixed oxides, we analyzed effects of oxygen vacancies introduced in the tetrahedral position. $Ce_{0.75}Zr_{0.25}O_{1.75}$ is a structure with 12.5% oxygen vacancy. Our calculated cohesive energies of $Ce_{0.75}Zr_{0.25}O_2$ and ($Ce_{0.75}Zr_{0.25}O_{1.75}$ + an oxygen) suggest that it will cost an energy of 11.73 eV to create an oxygen vacancy. Similarly, the difference in cohesive energies of CeO_2 and ($CeO_{1.75}$ + an oxygen) is 11.83 eV. To assess the mechanism suggested in one of the earlier investigations [11], we simulated a configuration of $Ce_{0.75}Zr_{0.25}O_2$, with one of the oxide ions displaced from the tetrahedral position to the octahedral vacant position. On relaxing the structure, we find that the oxygen moves back to the tetrahedral position, resulting in the original structure without vacancy and having the same energy. Thus, it rules out the possibility for an oxygen atom to occupy the octahedral site in the bulk form of these oxides. Figure 4(b) and (c) show the configurations with oxygen vacancies in the ceria-zirconia mixed oxide. Our calculations with oxygen vacancy in ceria-zirconia show that presence of oxygen vacancy makes the structure weakly bound and increases the number of weak oxygens, contributing to higher OSC.

Figure 5(b) shows the presence of both short and long bonds in vacancy introduced ceria as in $CeO_{1.75}$ compared to the single bond length of 2.36 Å in pure CeO_2. Presence of longer bonds compared to CeO_2, shows the availability of weaker oxygens in $CeO_{2-\delta}$. $Ce_{0.75}Zr_{0.25}O_{1.75}$ shows more prominant change of bond lengths and presence of longer bonds compared to $Ce_{0.75}Zr_{0.25}O_2$. In $ZrO_{1.75}$, longer bond lengths are

found compared to ZrO_2. Hence presence of oxygen vacancies is an important factor contributing to the OSC of mixed oxides (see table 5 for bond lengths in vacancy introduced mixed oxides). The values of the oxygen valencies for $Ce_{0.75}Zr_{0.25}O_{1.75}$ are given in table 4. In each case, the number of strong and weak oxygens are four and three, respectively. Hence it shows that the position of the tetrahedral vacancy was the site of an weakly bound oxygen.

4. Conclusion

EXAFS study of $Ce_{1-x}Zr_xO_2$ shows that oxygen coordination around Zr is $4+4$. The structures determined from our first-principles calculations agree with the EXAFS results. We find that the presence of short and long bonds result in two type of oxygens: strongly and weakly bound. The stronger ones have valency greater than 2.0 and the weaker ones have valency less than 2.0. Using the valencies of cations and oxygens calculated by bond valence method, we determined the weakly bound oxygens responsible for higher OSC in the mixed oxides. Presence of oxygen vacancies in ceria-zirconia has been found to result in longer cation-oxygen bonds, which might lead to weakening of strongly bound oxygens, thereby further increasing the OSC.

Acknowledgment

We thank the central computing facility at JNCASR for use of computational resources, UVW acknowledges a DuPont Young Faculty Grant, GD thanks UGC for research fellowship.

References

[1] A. Trovarell, Comment. Inorg. Chem. 20 (1999) 263.
[2] H.C. Yao and Y.F.Y. Yao, J. Catal. 86 (1984) 254.
[3] N.V. Skorodumova, S.I. Simak, B.I. Lundqvist, I.A. Abrikosov and B. Johansson, Phys. Rev. Lett. 89 (2002) 166601.
[4] M. Ozawa, M. Kimura and A. Isogai, J. Alloys Comp. 193 (1993) 73.
[5] G. Ranga Rao, J. Kaspar, R. Di Monte, S. Meriani and M. Graziani, Catal. Lett. 24 (1994) 107.
[6] P. Fornasiero, R. Di Monte, G. Ranga Rao, J. Kaspar, S. Meriani, A. Trovarell and M. Graziani, J. Catal. 151 (1995) 168.
[7] T. Masui, T. Ozaki, K. Machida and G. Adachi, J. Alloys Compd. 303–304 (2000) 49.
[8] C. de Leitenburg, A. Trovarelli, J. Llorca, F. Cavani and G. Bini, Appl. Catal. A: Gen. 139 (1996) 161.
[9] M. Alifanti, B. Baps, N. Blangenois, J. Naud, P. Grange and B. Delmon, Chem. Mater. 15 (2003) 395.
[10] T. Murota, T. Hasegawa, S. Aozasa, H. Matsui and M. Motoyama, J. Alloys Compd. 193 (1993) 298.
[11] E. Mamontov, T. Egami, R. Brezny, M. Koranne and S. Tyagi, J. Phys. Chem. B 104 (2000) 11110.
[12] G. Vlaic, P. Fornasiero, S. Geremia, J. Kaspar and M. Graziani, J. Catal. 168 (1997) 386.
[13] S. Lemaux, A. Bensaddik, A.M.J. van der Eerden, J.H. Bitter and D.C. Koningsberger, J. Phys. Chem. B 105 (2001) 4810.
[14] D.C. Sayle, S. Andrada Maicaneanu and G.W. Watson, J. Am. Chem. Soc. 124 (2002) 11429.
[15] K. Sohlberg, S.T. Pantelides and S.J. Pennycook, J. Am. Chem. Soc. 123 (2001) 6609.
[16] T.X.T. Sayle, S.C. Parker and C.R.A. Catlow, Surf. Sci. 316 (1994) 329.
[17] S. Fabris, S. de Gironcoli, S. Baroni, G. Vicario and G. Balducci, Phys. Rev. B 71 (2005) 041102(R).
[18] D. Vanderbilt, Phys. Rev. B 41 (1990) 7892.
[19] S. Baroni, A. Dal Corso, S. de Gironcoli and P. Giannozzi, http://www.pwscf.org
[20] http://www.library.cornell.edu/nr/bookcpdf/c10-7.pdf
[21] H.J. Monkhorst and J.D. Pack, Phys. Rev. B 13 (1976) 5188.
[22] I. D. Brown, in: *Structure and Bonding in Crystals*, Vol. II, eds. M. O'Keefe and A. Navrotsky (Academic Press, Inc. 1981) ch. 14, p. 1.
[23] M. O'Keffe and S. Hansen, J. Am. Chem. Soc. 110 (1988) 1506.